Chemistry–A European Journal

Research Article
doi.org/10.1002/chem.202200930

Chemistry
Europe
European Chemical
Societies Publishing

www.chemeurj.org

The Mechanism of Biochemical NO-Sensing: Insights from Computational Chemistry

Ahmed M. Rozza,[a, b] Marcell Papp,[a] Neil R. McFarlane,[c] Jeremy N. Harvey,*[c] and Julianna Oláh*[a]

Abstract: The binding of small gas molecules such as NO and CO plays a major role in the signaling routes of the human body. The sole NO-receptor in humans is soluble guanylyl cyclase (sGC) – a histidine-ligated heme protein, which, upon NO binding, activates a downstream signaling cascade. Impairment of NO-signaling is linked, among others, to cardiovascular and inflammatory diseases. In the present work, we use a combination of theoretical tools such as MD simulations, high-level quantum chemical calculations and hybrid QM/MM methods to address various aspects of NO binding and to elucidate the most likely reaction paths and the potential intermediates of the reaction. As a model system, the H-NOX protein from *Shewanella oneidensis* (So H-

NOX) homologous to the NO-binding domain of sGC is used. The signaling route is predicted to involve NO binding to form a six-coordinate intermediate heme-NO complex, followed by relatively facile His decoordination yielding a five-coordinate adduct with NO on the distal side with possible isomerization to the proximal side through binding of a second NO and release of the first one. MD simulations show that the His sidechain can quite easily rotate outward into solvent, with this motion being accompanied in our simulations by shifts in helix positions that are consistent with this decoordination leading to significant conformational change in the protein.

Introduction

The sole intracellular receptor for nitric oxide (NO) in humans is soluble guanylyl cyclase (sGC) – a heterodimeric heme protein consisting of alpha and beta subunits, each comprising four identifiable domains: The N-terminal H-NOX (Heme-nitric oxide/oxygen binding) domain, a Per-Arnt-Sim (PAS) domain, a coiled-coil signaling helix, and the C-terminal cyclase domain (Figure 1).[1] NO is a reactive free-radical diatomic molecule, and it functions in humans as a signaling molecule that mediates a broad range of physiological functions such as vasodilation, wound healing, neurotransmission, and response to infectious disease.[2,3] Pathological conditions like coronary artery disease, moyamoya disease, and hypertension are found to be associated with improper function of sGC due to genetic mutations,[4,5] thus it is a drug target for the treatment of pulmonary hypertension and chronic heart failure.[6] Furthermore, heme oxidation and dissociation have been shown to weaken NO-signaling in vivo, resulting in a number of pathological conditions. Various sGC stimulators and activators have been developed in order to enhance NO signaling, and the structural mechanisms by which the stimulator riociguat and the activator cinaciguat bind and activate the sGC enzyme have recently been resolved.[7]

NO signaling is initiated by the activation of NO synthases (NOSs), which generate NO endogenously by L-arginine oxidation to yield L-citrulline and NO.[6] Three isoforms of NOS expressed by three different genes can produce NO in the human body: eNOS (endothelia NOS-NOS3 gene), nNOS (neuronal NOS-NOS1 gene), and iNOS (inducible NOS-NOS2 gene). NO then diffuses across the membrane of the target cell without obstruction to bind to the heme group located in the β H-NOX domain of sGC. This, in turn, leads to the activation of the C-terminal catalytic domain, which catalyses formation of the second messenger molecule, cyclic guanosine monophosphate (cGMP), from guanosine triphosphate (GTP), resulting in the launching of various downstream signaling cascades – often known as the NO-sGC-cGMP pathway.[8] Uptake of NO results in 200-fold increase in cGMP production compared to the basal level, but binding of CO also leads to a few-fold increase. In contrast, sGC is entirely insensitive to oxygen, making it a NO-

[a] A. M. Rozza, M. Papp, Dr. J. Oláh
     Department of Inorganic and Analytical Chemistry
     Budapest University of Technology and Economics
     1111 Budapest Műegyetem rakpart 3. (Hungary)
     E-mail: olah.julianna@vbk.bme.hu

[b] A. M. Rozza
     Department of Biotechnology, Faculty of Agriculture
     Al-Azhar University
     Cairo 11651 (Egypt)

[c] N. R. McFarlane, Prof. J. N. Harvey
     Department of Chemistry
     KU Leuven
     3001 Leuven Celestijnenlaan 200 f- box 2404 (Belgium)
     E-mail: jeremy.harvey@kuleuven.be

Chem. Eur. J. 2022, 28, e202200930 (1 of 13)

© 2022 The Authors. Chemistry - A European Journal published by Wiley-VCH GmbH

Chemistry–A European Journal | Research Article
doi.org/10.1002/chem.202200930

Chemistry
Europe
European Chemical
Societies Publishing

Figure 1. (A) Quaternary structure of the β-subunit of sGC and the overall signaling process. Domain names are given in black and chemical reactions are shown in red. The model of the enzyme used in QM calculations and as the QM region of QM/MM calculations is circled in red – where needed, additional NO molecules were added to it in the calculations. (B) Proposed mechanism of sGC under exposure to NO. **A**, **B**, **C**, **D** and **D*** are the species of the proposed mechanisms. Apolar hydrogens and side chains of the porphyrin ring have been omitted for clarity. The axial histidine ring is represented by an imidazole ring.

sensor protein.[9] NO can also be generated exogenously from NO-donor compounds such as nitroglycerin (GTN), which is implied to be metabolized to NO in vivo by cytochrome p450 enzymes.[10] GTN is frequently used as a vasodilator in conditions of cardiovascular ischaemia.

The NO-sGC-cGMP pathway is mediated by a conformational change induced by NO binding to the heme group of the β-subunit H-NOX domain. In the resting state of the enzyme the central ferrous iron is five-coordinate and is in the high-spin state (Figure 1, species *A*). It is axially ligated to a histidine residue on the proximal side of the heme group.[11] Originally, the NO-sGC activation process was thought to result solely from a single NO molecule binding to the distal side of the heme iron resulting in the formation of a six-coordinate low-spin heme group (Figure 1, species *B*) followed by rupture of the Fe-His bond (Figure 1, species D*). Based on subsequent exper-

imental studies it has, however, been proposed that a single NO can only partially activate sGC and that an additional NO should be involved in the full NO activation mechanism.[12–14]

Although experimental studies implied that sGC underwent multi-step NO binding, still, the exact binding site of the NO molecule or molecules remained controversial. Marletta and coworkers found that in the presence of excess NO, S-nitrosylation of Cys^{122} of the β H-NOX leads to full activation of the enzyme.[3] In another study, however, S-nitrosylation of the same residue by a nitrosylating agent resulted in desensitization of sGC and loss of responsiveness to NO.[15] It is worth keeping in mind that the thiol-NO reaction does not take place anaerobically, and it is too slow under normal oxidative conditions in the human body to be a factor in the observed fast NO binding.[16,17] However, it may occur under physiological conditions of oxidative stress.[3]

Chemistry–A European Journal

Research Article
doi.org/10.1002/chem.202200930

Chemistry Europe
European Chemical
Societies Publishing

Subsequently, further experimental investigations indicated that the sGC heme iron itself could also be the locus of binding of the second equivalent of NO. This requires the preceding or concurrent fission of the Fe-His bond as shown in Figure 1B. The binding of NO as a proximal ligand was suggested to strongly depend on NO concentration and as a final product **D**, involving a five-coordinate heme group with proximal NO was hypothesized to be the predominant form of the maximally activated sGC. Conversion of **B** to **D** implies the formation of a very transient intermediate the "bis-NO-sGC quaternary complex" (**C**), which is extremely difficult to detect leaving the intricate details of the reaction mechanism elusive. Such a multi-step process of NO binding was found to occur in the highly NO-selective cytochrome c′ – a microbial protein from *Alcaligenes xylosoxidans* – using stopped-flow Fourier transform infrared (FTIR) spectroscopy.[18] This protein is smaller than sGC and can form a stable five coordinate complex with NO bound to the proximal face of the heme (PDB code: 1E85). A sub-family of cytochrome P450s called TxtE has been studied to investigate the presence of Fe(II)-nitrosyl intermediate as a part of its catalytic cycle of nitrating cyclic substrates such as, L-tryptophan.[19] Experimental results generated from stopped-flow spectroscopic analysis showed that the rate of NO binding to Fe(II)-thiolate of the TxtE protein is 2.5 slower than the binding of O_2. In addition, DFT calculations supported this finding, where O_2 binds first to form a Fe(III)-superoxo complex and NO later reacts with this species to give the active intermediate Fe(III)-peroxynitrite. In turn, this splits homolytically to yield Fe(IV)-oxo heme and a free NO_2 radical via a small free energy of activation. Thus, NO doesn't bind to the TxtE protein in the same way that H-NOX does. A similar family of heme-thiolate proteins which has been mentioned earlier in this section are NOSs. These also detoxify the excess amount of peroxynitrite anion; however, an Fe(III)-NO complex is the result of peroxynitrite activation instead of the oxoferryl complex.[20]

The bacterial homologs of the H-NOX domains of sGC have been thoroughly researched to gain valuable information on the characteristics of gas binding.[21] Bacterial H-NOX sensors are grouped into NO- and O_2-sensors based on their affinities to gaseous molecules. Using stopped-flow UV-Vis and MCD spectroscopy, the kinetic parameters of NO, CO and O_2 binding – k_{on}, k_{off} and K_D – have been determined for H-NOX proteins from various species.[22] One particular H-NOX protein, the *Shewanella oneidensis* H-NOX (*So* H-NOX), has been suggested to exhibit characteristics resembling sGC: a capacity to break the Fe-histidine bond upon exposure to NO leading to the same five-coordinate heme iron with proximal NO as final product (**D**), presumably formed via an equivalent unobservable intermediate (**C**). Such a similarity holds out the promise that this protein serves as a good model of human sGC.[22]

However, conclusions of a recent study appear to contradict the hypothesis involving the formation of (**C**).[23] Through the use of UV-Vis and EPR spectroscopy, *So* H-NOX was investigated under limiting and excess NO conditions, and in both cases the product seemed to be the monoligated NO complex with distal coordination (**D***). While the observed breaking of the iron-histidine bond emphasizes the similarity between sGC and *So*

H-NOX, it also reinitiates the debate on the activation mechanism and on the nature of the active species. Especially the events following the binding of the first NO molecule are disputable, whether the scission of the Fe-histidine linkage occurs independently or assisted by the binding of a second NO molecule, and which of **D*** or **C** (which could lead to the generation of **D**) are more easily accessible.

Spectroscopically, the various species shown in Figure 1B are typically identified using UV-Vis spectroscopy. In the resting state of the enzyme, the UV-Vis spectra are characterised by a Soret peak at ~430 nm and a single broad α/β peak at ~555 nm. These features are representative of a 5-coordinate ferrous heme. Upon binding of one NO equivalent, the Soret peak moves to ~400 nm and a shoulder at ~485 nm emerges.[24] However, an experimental challenge found in these systems is that active states **D*** and **D** present the same UV-Vis spectra. Bearing this in mind, for **D** to be formed, **C** must first be visited. Given **C** is predicted to be a short-lived intermediate, it is difficult to say unambiguously which active state is the most prominent.

In the absence of convincing experimental evidence computational tools can provide us valuable insights on the reaction mechanism of enzymes.[25–28] The description of bond-breaking and -forming processes requires quantum chemical calculations where the electronic structure of the molecules can be directly treated. Two major approaches have been followed in recent years, the cluster model and combined quantum mechanics and molecular mechanics (QM/MM) calculations. In the cluster model a small to medium sized model of the active site can be treated quantum mechanically,[29–33] and a great advantage of this approach is that versatile quantum chemical approaches can be used to study the system even allowing the usage of highly accurate methods such as coupled cluster calculations. On the downside, the effect of the protein environment is either neglected or considered by continuum solvation models. QM/MM methods enable us to directly include in our model the whole protein structure, although at a lower level. These calculations usually use semiempirical or DFT methods for the description of the quantum chemically treated region and many successful applications prove the potential of this approach.[28,34–38]

However, complex biomolecular systems such as sGC cannot be accurately described by simply modelling bond formation and breaking processes. Changes in electronic structure typically induce some conformational change which in turn gives rise to signaling. The conformational changes can be studied using molecular mechanics-based molecular dynamics (MD), where the dynamic behaviour of the whole protein is simulated in solvent. Therefore, in order to obtain a more complete picture of the overall signaling processes and to study how the different events are linked, usually a carefully selected set of techniques is required yielding insight into the various facets of the process.

In this work, we use the computational methods described above to explore key aspects of signaling by sGC and to assess possible reaction pathways in *So* H-NOX as a model of human sGC. We start by employing various quantum chemical methods

to assess the thermodynamics of the different structures shown in Figure 1B using a model system, consisting of an Fe-porphin ring (i.e., a porphyrin ring without sidechains), an axial imidazole ring representing the histidine sidechain and NO molecules, where appropriate. Next, starting from the crystal structures of **A**, **B** and **D** from *So* H-NOX,[39] molecular dynamics simulations have been used to address the following questions: (1) Does NO diffuse into the proximal pocket? (2) How does the tertiary structure change when the proximal His decoordinates upon rupture of the Fe-His bond? (3) Is the movement of the His into/out of the proximal pocket facile? Finally, coordination of the first and second equivalent of NO as well as decoordination of the His residue have been addressed using QM/MM calculations in a large model of the protein. Through these calculations, we aim to gain insight into the core questions of *So* H-NOX activation related to NO-binding, and to resolve the following questions: (i) Is it plausible that a second NO equivalent binds to heme yielding intermediate **C**? (ii) Are pathways to **C** and **D*** energetically accessible starting from the NO-unbound structure **A**? (iii) Of **C** and **D***, which is the most easily accessible? All of the computational data generated herein is then used in conjunction with estimated physiological concentrations of NO gas to reach a conclusion about the favoured pathway.

Results and Discussion

QM calculations

While a number of previous studies have modelled bonding of NO to the imidazole-ligated heme group (**B**) with quantum chemical methods,[40–45] for consistency and in order to obtain near-benchmark quality results, a new set of calculations was performed. This work included a broad overview of DFT energies with different functionals, as well as some CCSD(T) calculations using the DLPNO-CCSD(T0) local correlation approach and the same basis set which, despite known caveats about accuracy,[46,47] should provide a reasonable benchmark for the DFT methods. Only results obtained with the ZORA-def2-TZVP basis set on all atoms are presented for consistency between DFT and DLPNO-CCSD(T0) calculations. We start by considering the spin state of the ground state of the studied model complexes (**A**, **B**, **C** and **D/D*** depicted in Figure 1B), followed by the discussion of the overall energy changes associated with NO and histidine coordination to the heme group.

Firstly, it is important to establish the electronic ground states of the species shown in Figure 1B. The ground state of **A** is a high-spin quintet which can react in a fast, almost barrierless spin-forbidden reaction with NO to yield **B**, which has a doublet ground state.[45,48] As in previous work,[45] we find the quartet and sextet states of **B** to lie higher in energy. **C** is an elusive intermediate and as such there is no experimental data available on its ground spin state. Using the BP86-D3 functional, **C** is predicted to have a singlet ground state lying 16.7 kcal/mol below the triplet, while the hybrid functionals predict close-

lying triplet and singlet states, the triplet being more stable by 2–3 kcal/mol. These findings are not unusual as it has been found that gradient corrected methods such as BP86 tend to favour low-spin states, while hybrid functionals often yield small energy differences between high- and low- spin states.[49,50] Bearing this discussion in mind, due to the minimal energy difference found with hybrid functionals, **C** was modelled in the singlet state. Decoordination of the imidazole ring gives **D/D***, which has a doublet ground state according to a DFT study conducted by Parrinello et al.[51]

Let us turn our attention to the relative energies of the studied species (Table 1). Our initial structure, **A**, is the relative energy baseline from which other energies are calculated. In QM calculations with a small model, **D** and **D*** are the same species, as the protein environment is not taken into account, so are considered as one in the following discussion.

Inspection of the data in Table 1 gives information on two important aspects: (1) how comparable are the results obtained with various DFT functionals with CCSD(T)? If the results are similar, we can have a larger confidence in trusting the conclusions drawn from them. (2) What kind of chemistry related to sGC activation do the obtained numbers suggest? It is first clear that, not including the CCSD(T) predicted data, the predicted energy change for the endothermic dissociation of imidazole from **B** to yield **D*** is fairly consistent for all functionals. The computed relative energies for substituting imidazole by NO (going from **B** to **C**) vary more significantly, with the hybrid functionals predicting an uphill process, while BP86-D3 finds this step to be exothermic, implying very strong binding of the second NO molecule. Unsurprisingly, given the lower admixture of exact exchange, B3LYP*-D3 yields a result closer to BP86-D3 than do the other two functionals. The CCSD(T) relative energies do not perfectly match those obtained with any of the functionals, but bearing in mind the expected inaccuracies in DLPNO-CCSD(T) for open-shell systems,[46,47] there is acceptable agreement with B3LYP–D3 and B3PW91-D3, so most of our discussion below will focus on results with these functionals. The BP86-D3 functional agrees much less closely, and we conclude that the predicted high stability of species **C** with this functional is an artefact.

Looking now at the predicted chemistry, NO binding to Fe(II) heme is energetically favourable, but being aware of the unfavourable entropic contribution not included here, binding is still predicted to be reversible, especially for low NO concentration. Next, dissociation of the imidazole group to yield

Table 1. QM relative energies (kcal/mol, including the ZORA Hamiltonian with the ZORA-def2-TZVP basis set) for all structures studied herein – **A**, **B**, **C**, and **D/D***. The relative energy changes for the two reaction pathways which are examined in more detail using QM/MM methods are also shown.

| Method | E_{rel} (kcal/mol) | | | | ΔE_{BC} | ΔE_{BD^*} |
	A	B	C	D/D*		
BP86-D3	0.0	−56.6	−62.9	−41.4	-6.3	15.2
B3LYP–D3	0.0	−22.2	−6.7	−8.6	15.4	13.5
B3LYP*-D3	0.0	−32.7	−24.0	−18.0	8.7	14.7
B3PW91-D3	0.0	−24.5	−9.7	−8.7	14.8	15.8
DLPNO CCSD(T)	0.0	−13.3	3.3	5.9	16.7	19.3

Chemistry–A European Journal

Research Article
doi.org/10.1002/chem.202200930

Chemistry Europe
European Chemical
Societies Publishing

D is somewhat endothermic, but the energy change is relatively modest, consistent with relatively facile dissociation of the histidine sidechain from intermediate **B**. Finally, with the exception of BP86-D3, coordination of a second NO group to yield **C** (i.e. transition from **B** to **C**) is endothermic. This prediction is consistent with all hybrid functionals and with DLPNO-CCSD(T) so even allowing for the errors in these methods, we consider that **C** is unlikely to be formed as a stable species in sGC and related systems, especially considering the unfavourable entropy of binding (not included in the relative energies of Table 1) and the low physiological concentration of NO of 100 pM – 5 nM.[52] As **C** lies slightly lower in energy than **D/D***, it does however represent a plausible intermediate in an exchange process that would convert **D*** to **D**.

MD simulations

Before analysing our MD trajectories for various properties related to our stated goals in the **Introduction**, we assessed the stability of the MD simulations for **A**, **B**, **D***, and **D** by measuring the RMSD of the protein's mainchain. Table S1 in the Supporting Information shows the average values of the RMSDs, which range from 0.12 to 0.16 nm. This deviation from the reference structure (i.e. the zero ns structure) appears to be acceptable, demonstrating the inherent protein flexibility. We also calculated the cumulative average of RMSD, as shown in Figure S1B in the Supporting Information, where flattened curves can be seen.

NO Diffusion Process

NO binding by heme proteins involves two key stages: (1) ligand diffusion to the active site (2) bond formation between the ligand and the Fe(II)-heme protein, whose description requires fundamentally different approaches.[45] In the previous section (as well as the upcoming **QM/MM Calculations**), we dealt with the latter, let us now consider the diffusion process.

In order to properly model ligand diffusion into proteins, long MD simulations are needed where the diffusion events from the solvent phase into the active site and vice versa are well-equilibrated. Therefore, we carried out a 400 ns MD simulation of **A** with 40 NO molecules to examine the probability of NO diffusion into both distal and proximal pockets. The distal pocket is surrounded by residues: Met[1], Ile[5], Leu[73], Leu[138], Cys[141], and Leu[145]; while the proximal pocket is defined by residues: His[103], Asn[107], Ser[114], and Pro[116]. Based on Table 2 – that provides a general overview of some characteristic properties of NO diffusion into each pocket – we compared these properties of *So* H-NOX with other NO-sensing bacterial H-NOX systems studied for NO diffusion.[52] The average time that NO can occupy the distal pocket of *So* H-NOX was found to be significantly shorter than that of *Nostoc sp.* H-NOX (920 ps) but of the same order of magnitude as *Kordia algicida* (116 ps). At the same time, the percentage of the distal pocket occupancy with NO was observed to be reasonably comparable

Table 2. Ligand-binding properties of the distal and proximal pockets derived from 400 ns long MD simulations of **A**.

Binding Pockets	Distal	Proximal
Average time trapped[a]	58.2 ps	9.7 ps
Number of in-and-out events[b]	6358	6975
Occupancy with at least one NO molecule[c]	90.5%	16.6%
Maximum number of gas molecules[d]	3	1

[a] The average amount of time that NO gas molecules spent inside a given pocket before exiting again. [b] The number of in-and-out diffusion events made by NO gas molecules, where "protein core→geminate pair" represents the in-event path, and the reversible direction of this route represents the out-event path.[45,53] [c] Occupancy of the pockets with at least one NO molecule during the simulation time. [d] Maximum number of NO gas molecules found inside both pockets over the course of the MD simulation.

between these three H-NOXs. On the other side, NO was trapped within the proximal pocket of *So* H-NOX for a seemingly shorter time than in both *Nostoc* and *Kordia*, 212.2 ps and 7940 ps, respectively, with a much lower number of in-and-out-events in the two H-NOXs. The same pattern was seen for the occupancy percentage with at least one NO molecule being inside the proximal pocket, which could be attributed to the availability of the tunnelling system discussed later in this section.

In our simulations, NO molecules tend to smoothly diffuse into the distal pocket and at least one of them is present there during most of the simulation time, sometimes indeed with more than one NO present (Table 2). The proximal pocket, on the other hand, is only ever occupied by one gas molecule at a time, and this for only 16% of the MD trajectory. Thus, NO appears to be able to enter both pockets, so that reaction from both sides might occur, though geminate recombination in the distal pocket, which is expected to be barrierless, should be more facile. Indeed, in a previous experimental study on sGC using time-resolved spectroscopy,[54] the timescale for NO rebinding from the protein core to a 5-coordinate His-bound heme group (i.e. to **A**) was found to be as short 6.5 ns.

We also inspected the tunnelling system that the gas ligand uses to access the distal and proximal pockets. After visually scrutinizing the inward/outward migration events of the gas ligands (i.e., from the solvent to the protein matrix and finally the pocket to the protein matrix then to the solvent environment), one short route was recognized. This tunnel was observed to be most likely taken by the gas molecules to first reach the distal pocket and then bounce horizontally over the heme distal face towards a cavity next to the heme (shown in purple mesh, Figure 2) that lies between helices αA, αG, and αF, leading to the proximal pocket. Only one of the 40 NO gas molecules found that pathway into the proximal pocket, and because there was no simple exit pathway, it remained in the proximal pocket (and no other NO molecules exchanged positions with it). We propose that this is due to the apparent short length of the tunnel, and the fact that the majority of NO molecules stream through it, making it occupied the majority of the MD simulation time. Helices αC, αD and αG line this short tunnel (the orange mesh representation shown in Figure 2),
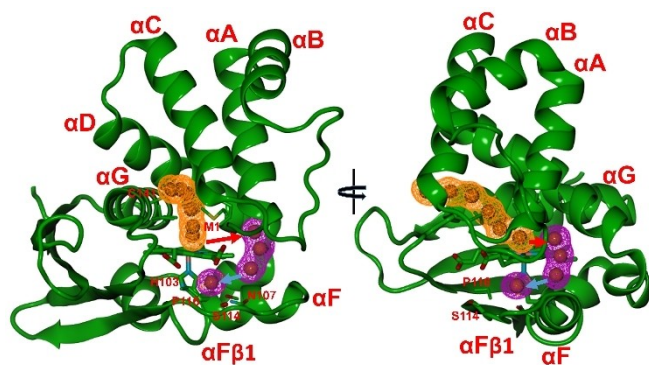
Chemistry–A European Journal

Research Article
doi.org/10.1002/chem.202200930

Chemistry Europe
European Chemical
Societies Publishing

Figure 2. Identified gas migration tunnels towards the distal and proximal pockets in *So* H-NOX protein. The orange mesh depicts the tunnel that transports the NO gas molecules from the external solvent environment to the protein matrix and finally to the distal pocket. The red and light blue arrows show the movement of NO gas molecules from the distal face to the proximal pocket which is represented by purple mesh.

allowing the gas ligands to move directly from the external solvent environment to the vicinity of the heme propionate sidechains and subsequently to heme-Fe (i.e., the iron ion coordinated to the porphyrin). This tunnel has been observed as the shortest route in two other bacterial H-NOX proteins from Nostoc sp. and Caldanaerobacter subterraneus, making it highly selective and typical molecular tunnel in H-NOX proteins.[53,55] In addition, we found another longer access tunnel (between helices αA and αD) that gas molecules only rarely used to migrate to the distal pocket. Previously, we identified a third tunnel in H-NOX proteins,[53] however, it is blocked by two aromatic amino acids (His^{81} and Tyr^{110}), which form a steric barrier mostly preventing NO molecules from diffusing into the H-NOX protein matrix. These amino acids sit opposite to each other, and have a high possibility for hydrogen bonding to be established between them.

Proximal Histidine Swing-Out

As discussed in the Introduction, dissociation of the histidine proximal ligand from the heme group to generate **D*** or **D** is known to allow the proximal histidine to move away from the heme partner, and to be able to lead to pronounced structural changes that are believed to be important for signal transmission between sGC domains. A crystal structure for **D** confirms this conformational change. However, the position of the proximal histidine is unknown in the case of the distal NO complex **D*** for which no crystal structure exists so far.[23] What is also unknown is the ease with which the protein changes conformation upon His^{103} decoordination, and the relative free energy of the "inward" and "outward" conformations of the His^{103} sidechain, in which it is respectively "close" and "distant" to the heme group. In this context, MD trajectories of **D*** and **D** complexes (which differ in whether the NO ligand is attached to the distal or proximal side of the heme group) were thoroughly investigated for the motion of the proximal histidine after

dissociation from the proximal face of heme; how it affects the proximal subdomain of H-NOX protein; and its favourable location in both states.

MD simulations for **D*** and **D** complexes show closely similar behaviour for the motion of the proximal Histidine. Along the simulation trajectory of both complexes, two distinct conformations (inward & outward) for the proximal His^{103} were observed, and the swinging between the two positions was thermally accessible. The outward conformation was found to be the dominant state in **D** and **D*** complexes, but the inward conformation was also seen in a non-negligible portion of the simulations. Figure 3 shows the transition events between the two conformations, which are represented by a change in $Fe-His_{\varepsilon N}^{103}$ distance over the simulation time. We can also clearly see that at an early stage of both complexes' simulations, the transition from inward to outward in **D***- or from outward to inward in **D** took nearly the same amount of time (~50 ns). Then, for the next 100 ns of the simulation of **D**, the transition occurred four times, with an average of 11 ns of being trapped in the inward conformation. In the **D*** simulation, on the other hand, the His sidechain remains in the outward position, with no further transitions.

The two locations of the proximal histidine in both NO-bound forms were visually investigated to identify the set of interactions within each conformation: (a) Histidine was observed to be in the heart of the proximal pocket (inward) – with an average $Fe-His_{\varepsilon N}^{103}$ distance of ~7.5 Å – due to rotation of the αF helix followed by motion of the αFβ1 loop (Figure 4A), with an average dihedral angle of ~ −79° around $C_\alpha - C_\beta$ (χ_1) bond of His^{103}. The rotation of the His^{103} imidazole ring may also contribute to the inward displacement. Upon His^{103} decoordination, the imidazole ring of His^{99} rotates outward to the solvent area, eliminating the H-bond between the carbonyl oxygen of His^{99} and H-δN of His^{103}, allowing the His^{103} side chain to move freely. This is obviously seen in the **D*** simulation (see Figure S4B in the Supporting Information), where the His^{103} was in closer contact than in the initial conformation of **D**. Thus, the side chain of His^{103} may be positioned away from the heme proximal face, and instead within plausible hydrogen-bonding distance of either or both of Ile^{98} or Ile^{118}, (δN-Hof His^{103} with carbonyl oxygen "O=C" of Ile^{98} & εN of His^{103} with amide hydrogen "H–N" of Ile^{118}) (see Figure S3A & B in the Supporting Information); (b) Swinging-out to the solvent-accessible void (outward), which, as was shown above, appeared to be the most favourable position for the proximal His^{103} (Figure 3A and Figure 4A), and corresponds to its position in the crystal structure of **D**.[39] The "swinging out" motion is associated with change in the dihedral rotation around the $C_\alpha-C_\beta$ bond (χ_1) by ~90° from the inward state[39] – which was characterized by an average torsion angle of ~ −169° – and with rotation of the αF helix, which leads to changes in positions of the backbone atoms of the proximal histidine by ~1 Å. Consequently, the side chain of His^{103} was then trapped in a new set of polar interactions with Asn^{107}, His^{99}, and water molecules (see Figure S4A, B in the Supporting Information). This group of interactions is noticeably wider than the set established in the inward location, which could be considered as the primary key
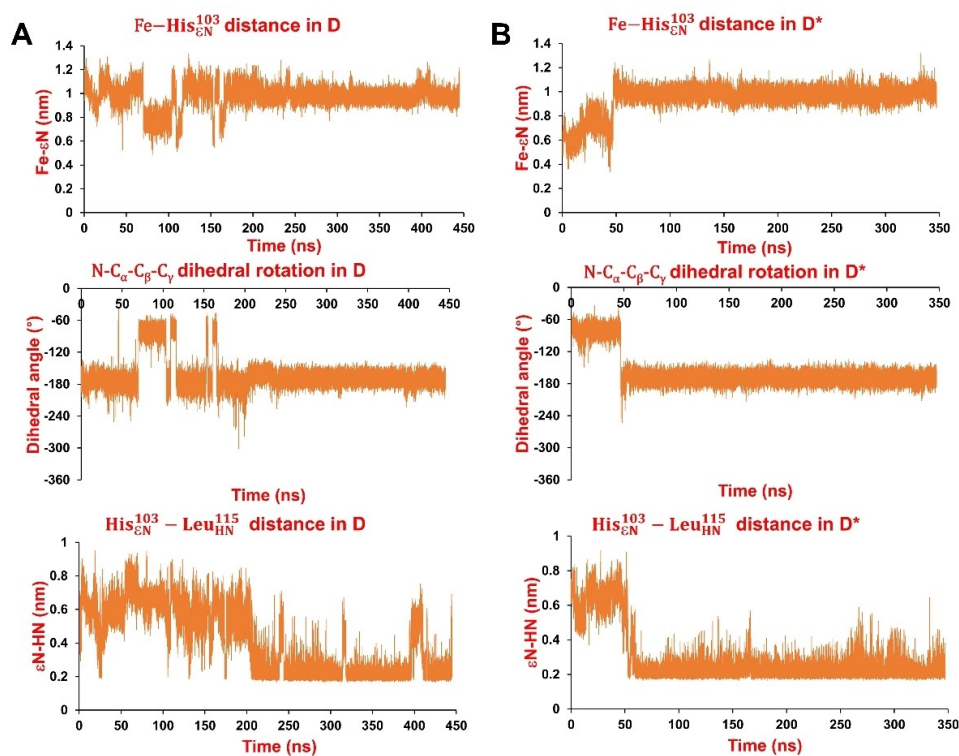
Chemistry–A European Journal

Research Article
doi.org/10.1002/chem.202200930

Chemistry Europe
European Chemical
Societies Publishing

Figure 3. Time evolutions (ns) of the calculated distances (nm) and dihedral rotation around C_α–C_β bond in both complexes (A) **D** and (B) **D***. The distances are between εN of His[103] and both heme-Fe & amide hydrogen of Leu[115]. The N–C_α–C_β–C_γ dihedral angle of His[103] is calculated in both **D** and **D***.
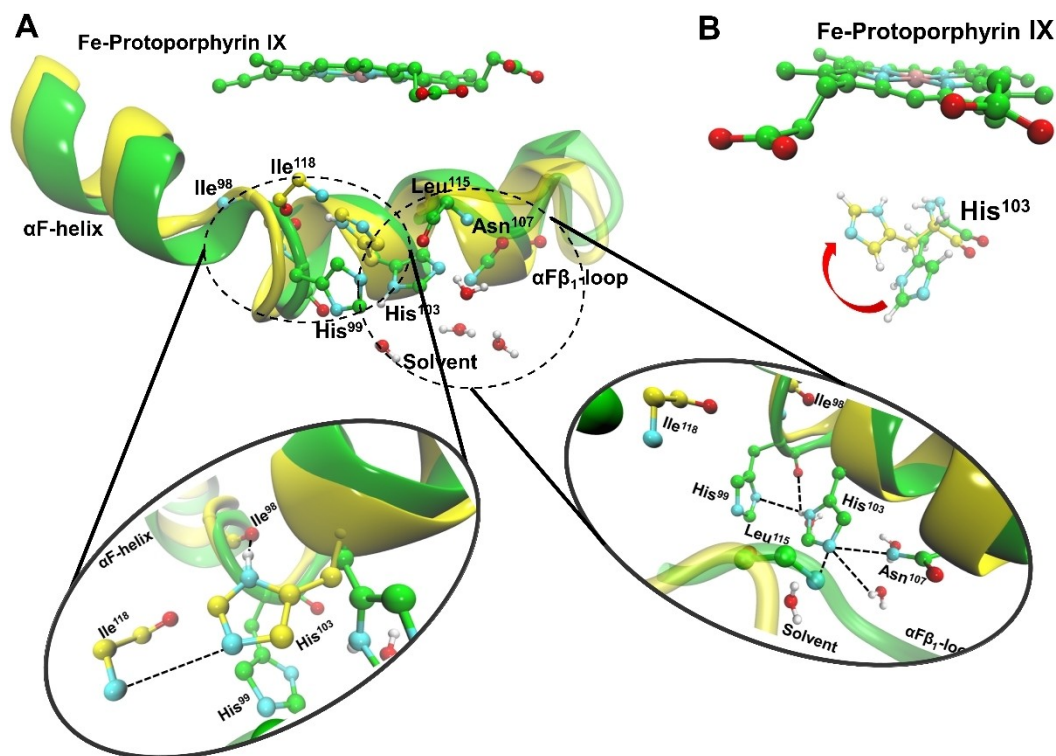
Figure 4. (A) Structural fluctuations of the proximal subdomain (αF-helix & αFβ$_1$-loop) between the inward (helix, loop, and carbon are coloured in yellow) and the outward (helix, loop, and carbon are coloured in green) conformations – It shows the hydrogen bond network in both states. (B) Shows the rotation the dihedral around C_α–C_β bond of the proximal His[103].

Chemistry–A European Journal   Research Article
doi.org/10.1002/chem.202200930

Chemistry
Europe
European Chemical
Societies Publishing

to the stabilization of the outward conformation for the majority of the simulation time. The rotation of the αF helix also could aid in the formation of an H-bond between the carbonyl oxygen of Asp[100] and the amide hydrogen of Leu[104], which might keep the histidine side chain to be exposed to the solvent area, and this has previously been shown in a study on the same system.[39] While histidine was in the outward state, we observed another H-bond that may establish an interaction between αF helix and αFβ1 loop, particularly between the εN of His[103] and the amide hydrogen of Leu[115] (Figure 3A & B and Figure 4A). Given the presence of the PAS domain – which is adjacent to the H-NOX domain in the human sGCα1β1 heterodimer – the outward state of the αF-helix and αFβ1-loop of the H-NOX domain may cause a steric clash with the PAS domain's sidechains at the domain-domain interface, necessitating structural rearrangement to accommodate the conformational change of the β1 H-NOX. This was demonstrated by superimposing the NO-bound β1 H-NOX domain onto the inactive state cryo-electron microscopy structures.[56]

Overall, the fluctuation between the inward and outward states of the histidine side chain was found to occur on a relatively short timescale. This conclusion is consistent with the short time constant (70 ps) that has been observed for the rebinding step of the proximal Histidine to the proximal face of the heme moiety in sGC.[54] This short timescale might be interpreted as corresponding to the easiest route for return to the starting species (**A**) from either **D*** or **D**, but this assignment will be discussed later following the description of the QM/MM calculations.

QM/MM Calculations

We next consider the predicted energies for bonding and dissociation events at the heme group, based on new QM/MM calculations and on reference to previous[45] QM calculations and those reported here (see *QM Calculations*). Geminate binding leading from **A** to **B** was predicted to be facile once the NO ligand is present in the distal pocket in previous work[45] and has not been considered again here. Here we primarily focus on whether dissociation of the proximal histidine occurs directly (thus **B** to **D***) or is assisted by the coordination of a second NO molecule on the proximal side of the heme (**B** to **C**). Both of these processes were predicted to be endothermic by QM calculations, the present QM/MM calculations aim to investigate their feasibility in the protein environment.

To study the pathway from **B** to **D***, any changes in electronic spin should first be considered. In this case, both **B** and **D*** are found to have a doublet ground state, so the transition is formally spin allowed. To generate reaction pathways, adiabatic mapping procedures were performed on three starting structures of **B** using BP86-D3 and B3LYP–D3 to describe the QM region. While the BP86 functional is not overall very accurate for sGC energetics, it does reproduce the relative energy of **B** and **D/D*** quite accurately so can be used here. Average bond lengths of reactant and product structures obtained from mapping procedures with both methods are

given in Figure 5(I). Turning our attention first to BP86-D3, the changes in bond lengths tell a relatively simple story whereby d(Fe-NO$_{distal}$) remains unchanged at ~1.70 Å and d(Fe-IM) lengthens from 2.50 Å to a non-bonded distance of 4.30 Å. These bond length changes can be interpreted as the Fe-IM bond breaking, without changing d(Fe-NO$_{distal}$) to any significant degree. The BP86-D3 and B3LYP–D3 predicted structures are also very similar to one another, with the only noteworthy difference being a slight increase in d(Fe-NO$_{distal}$), but this is comfortably within expected error margins. In both methods, this is in accordance with what is expected to happen in this reaction pathway, and the changes in bond lengths agree favourably with previous QM/MM studies on a related system.[45] Moving now to the energy changes associated with these conversions, energy profiles from both methods show no additional barrier above their endothermicity, and accordingly, we do not find local minima for the product, **D***. Hence the predicted relative energy of this species depends in a somewhat arbitrary way on the point along the calculated dissociation curves chosen to correspond to "product". Using a distance of 4.3 Å, we find **D*** to lie 17.2 and 19.1 kcal/mol above **B** with BP86-D3 and B3LYP–D3, respectively, as compared to 15.2 and 13.5 kcal/mol obtained in the QM calculations, respectively. These findings are as we would expect, given that it was found in the *QM Calculations* that BP86-D3 could compare to the more accurate methods quite agreeably when modelling the change from **B** to **D/D***. Energy profiles explicitly showing the QM and MM contributions with associated structures for these calculations, as well as reactant and product structures for all snapshots with the comparison between levels of theory can be seen in the Supporting Information.

Dissociation of His leads to a five-coordinate heme group with a distal NO ligand, **D***. We propose that this could convert to **D** via **C** by entrance of a second NO ligand in the proximal pocket, binding of NO and dissociation. These steps have not been considered in detail, but we assume that given the relatively low energy of the putative **C** intermediate in the QM calculations, this inversion could occur relatively easily. This conclusion is also supported by QM/MM calculations on a
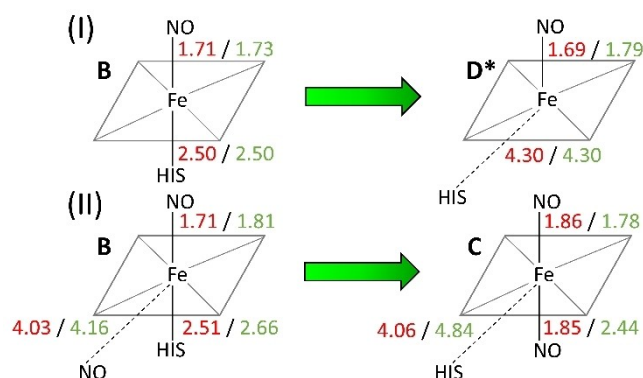

Figure 5. Average bond lengths of reactant and product structures for QM/MM modelling of the transition from (I) **B** to **D***, and (II) **B** to **C**. In red are the bond lengths associated with BP86-D3 modelling, and in green are those associated with B3LYP–D3 modelling.

Chemistry–A European Journal

Research Article
doi.org/10.1002/chem.202200930

Chemistry
Europe
European Chemical
Societies Publishing

possible direct route from **B** to **C** – see below. Of course, to a first approximation, neglecting interactions with the protein environment, **D*** to **D** conversion should be thermoneutral, but considering these interactions, one of the two may in fact be somewhat favoured in the protein. Given that there are experimental crystal structures of **D** but not of **D***, presumably the former is more stable.

We have also used QM/MM calculations to investigate the pathway leading from **B** to **C** upon binding of a second NO equivalent. In this case, the starting structure of **B** has an additional NO ligand added in the proximal pocket. Inclusion of the additional NO means that the starting structure now has two possible ground states: a triplet or an open-shell singlet. As it was found in the *QM Calculations* that the singlet and triplet states of **C** with two bound NO ligands lie very close in energy, we chose to consider the reaction pathway in the singlet state only. As the reaction progresses from **B** to **C**, the obtained electron distribution changed from an open-shell singlet to a closed-shell singlet. The spin population of atoms was continuously monitored, and great care was taken to locate the lower-lying of the open-shell and closed-shell states at each point, in order to get a smooth reaction profile. As previously, to generate reaction pathways, adiabatic mapping procedures were performed using a BP86-D3 or B3LYP–D3 description for the QM region. In both cases, the reaction was followed by constraining a reaction coordinate corresponding to the difference between the two proximal Fe-ligand distances. It is worth noting that the constraint used is different to that used in the study of the route leading from **B** to **D*** and allowed more degrees of freedom. The average bond lengths of reactant and product structures using both methods are given in Figure 5(II). As it does not directly participate in the reaction, $d(Fe-NO_{distal})$ is expected to change relatively minimally – as was observed in the **B** to **D*** pathways. In this case, $d(Fe-NO_{distal})$ changes from averages of 1.71 Å to 1.86 Å for BP86-D3, and 1.81 Å and 1.78 Å for B3LYP–D3. Particularly for BP86-D3, the change is more notable. The exact reason for this increase is not clear, but it is, overall, a relatively small change so is assumed to have a negligible effect on the reaction pathway. When using BP86-D3, $d(Fe-NO_{prox.})$ converges to an average distance of 1.85 Å, which is relatively similar to $d(Fe-NO_{distal})$. On the other hand, with B3LYP–D3, $d(Fe-NO_{prox.})$ converges to an average bond length of 2.44 Å – significantly greater than $d(Fe-NO_{distal})$. This effect could be a result of the constraint used in this pathway, which allows simultaneous variation of both $d(Fe-NO_{prox.})$ and $d(Fe-IM)$, so long as the difference between them remains the same. Given this fact, it is plausible that the energy decrease associated with moving the histidine further away from the metal centre is greater than bringing the proximal NO closer, so the constraint choice may not be entirely suitable, here. Notwithstanding the above discussion, overall, the changes in bond lengths along the reaction paths make chemical sense and, on the whole, align well with the expected reaction scheme. The changes in bond lengths obtained with BP86-D3 and B3LYP–D3 (for details, please see the Supporting Information) show some degree of similarity, albeit not as much as in the case of the route from **B** to **D***. Considering now the relative

energy changes, when using BP86-D3, there is an energy barrier of around 6.4 kcal/mol. For the case of B3LYP–D3, the corresponding step was found to have no additional barrier above the endothermicity. Therefore, much like in the case of **B** to **D***, defining when the product has been reached is somewhat arbitrary. Here, we assumed this to occur once $d(Fe-NO_{prox.})$ stopped changing to any significant degree. The relative energy changes for the transition from **B** to **C** are −1.1 and +10.2 kcal/mol for BP86-D3 and B3LYP–D3, respectively. These QM/MM calculated reaction energies agree in broad terms with those obtained from the *QM calculations*, where the same process is predicted to have an energy change of −6.3 and 15.4 kcal/mol for BP86-D3 and B3LYP–D3, respectively. Energy profiles explicitly showing the QM and MM contributions with associated structures for these calculations, as well as reactant and product structures for all snapshots with the comparison between levels of theory can be found in the Supporting Information. As discussed in the context of the QM results, the B3LYP–D3 results are considered to be more accurate, so conversion of **B** to **C** is most likely endothermic, with a reaction energy similar to that for conversion of **B** to **D***. Based on these QM and QM/MM energies, and given the fact that NO binding to form **C** is entropically unfavourable (an effect not included here), we consider that formation of **D*** should be more favourable than formation of **C**. However, **D*** can most likely convert to **D** with **C** as intermediate.

Considering now the overall process in the protein, in presence of NO, **A** can be expected to convert ultimately to **D**, which is accompanied by histidine dissociation. Under low NO partial pressures, with the fact that **D** is similar in stability to **A**, **D** and **D*** are expected to slowly convert back to **A**. Conversion of **D*** back to **A** should be straightforward, simply involving recoordination of the histidine sidechain and dissociation of NO.[45] On the other hand, conversion of **D** to **A** in the absence of excess NO should be less facile as NO is required to enable the initial conversion of **D** to **D***. No other route leading from **D** to **A** is apparent, so at low NO partial pressures, conversion of **D** to **A** is predicted to be slow.

Overall Findings

Based on these QM, MD, and QM/MM results, and on their confrontation to experimental observations, we would hereby like to suggest an overall scenario for the chemical and conformational changes occurring upon interaction between NO and sGC.

For this discussion, it is useful to consider the relevant physiological concentrations of NO gas leading to switching signaling 'on' and 'off'. As previously stated, NO is synthesized by the NO synthase complex in endothelial cells and diffuses into neighboring smooth muscle cells, where it binds the heme group of the H-NOX domain to activate the sGC receptor, leading to cGMP accumulation. Oxidation of heme group or heme loss can cause NO insensitivity, and this can also be seen as an outcome of heterodimer dissociation.[57] Based upon an assortment of data, it has been suggested that the physiological

concentration of NO gas varies in the range of 100 pM–5 nM.[52] This is consistent with previous studies of the activity of sGC under increasing concentrations of NO,[58] with the corresponding activity plots showing simple saturation behaviour, which we interpret as meaning that sGC binds only 1 gas equivalent in the final activated state. It should also be noted that the activity reaches saturation at approximately 10 nM, similar to the upper bound of the proposed physiological concentration. Higher NO concentrations may occur in different cell types under oxidative conditions, such as leukocytes, endothelial cells, cardiac myocytes, nerve cells, and fibroblasts.[6] This, in turn, stimulates the expression of cytosolic iNOS to produce high level of NO. Following that, the excess NO level reacts with superoxide at a diffusion-controlled rate – surpasses the superoxide dismutase enzyme – resulting in the formation of the peroxynitrite anion, which causes cell toxicity.[59]

The initial route followed upon NO reaction with sGC certainly involves NO binding to form six-coordinate intermediate **B**. Given the relatively low binding energy, and the entropic cost of binding, however, as the partial pressure of NO drops, the thermodynamics of binding will become less favourable and dissociation to regenerate **A** and NO occur, with the balance presumably tipping to one side or the other as the NO concentration varies from the low to high ends of its physiological range. Species **B** also has a relatively low binding energy for the imidazole sidechain of the proximal histidine, so that decoordination of this group to yield initially **D*** should be feasible. Our MD simulations show that the His sidechain in **D*** can quite easily rotate outward into solvent, with this motion being accompanied in our simulations by shifts in helix positions that are consistent with this decoordination leading to significant conformational change in the protein. The timescale of our simulations as well as the size of the modelled system do not enable us to address this large-scale conformational change in full detail, but the role of the NO-binding induced His decoordination in 'triggering' it is supported by the present results.

In principle, NO could also bind to the heme group on the proximal side, leading to conversion of **B** to the bis-nitrosyl species **C**. Both the DFT QM calculations and the benchmark CCSD(T) results however show that NO binding in species **C** is relatively weak, which, together with the corresponding entropic cost, suggests that this species will not be formed as a stable intermediate in sGC at physiological concentrations of NO.

Our calculations also suggest a possible role for **D**, with a five-coordinate heme group and a proximal NO ligand. This could be accessed from **D***, in presence of elevated NO partial pressures, through diffusion of a second NO ligand into the proximal pocket and exchange through **C**. In this exchange process, as mentioned above, **C** is not suggested to be a stable long-lived species but is stable enough to be a plausible intermediate en route to **D**. The existence of a crystal structure of **D** suggests that the inversion process from **D*** to **D** may be somewhat thermodynamically favourable. The relevance of this conversion is as follows: while the intermediate **D*** can readily convert back to the resting state, **A**, through reversal of the

conformational change, rebinding of the proximal His sidechain, and NO dissociation, there is no such facile route for conversion of **D** to **A**. Hence at low NO partial pressure, **D*** would become thermodynamically disfavoured and should disappear. On the other hand, if the exchange from **D*** to **D** can take place during the period of elevated NO concentration associated with signaling, then reversal to the resting state, **A**, will become much slower, because at low NO concentration, **D** can only switch rather slowly to **D***, presumably again through **C**.

Conclusion

Gas-molecule mediated signaling is key to the proper functioning of organisms. Soluble guanylyl cyclase is the sole receptor of nitric oxide in the human body, and it contributes to versatile physiological processes. Although it has been thoroughly investigated experimentally and is an important drug target, there has been a long-standing debate on its reaction mechanism.

Using a combination of computational chemistry tools (quantum chemical calculations, molecular dynamics simulations and hybrid QM/MM calculations) and the *So* H-NOX model protein we suggest that after the initial binding of NO to the distal side of the heme group the iron-histidine bond undergoes facile scission and a 5-coordinate heme-NO species (**D***) is formed. The decoordination of histidine is facilitated by its rotation outward to the solvent and leads to slight changes in the tertiary structure of the protein. Under elevated concentrations of NO (i.e., during signaling) the distal five-coordinate heme-NO complex could be converted via the energy-rich bis-NO-heme intermediate (**C**) to the five-coordinate proximal heme-NO adduct (**D**). This species (**D**) with proximal-NO coordination may be thermodynamically somewhat more stable than **D*** and may be the major species involved in signaling due to its slower conversion back to the resting state of the enzyme (**A**) compared to **D***.

Computational Details

QM Calculations

A Fe-porphin model of the heme ring was used to model species **A**, **B**, **C**, and **D/D*** (in the reduced model, these two species are identical) in vacuum. Structures were optimized with the Gaussian 16[60] program package employing the B3PW91 functional with Grimme's D3 dispersion correction[61] and the BJ damping function[62] together with the $6-311+G^*$ basis set on Fe and the axial NO ligand(s), and the $6-31G^*$ basis set on all other atoms (please see the Supporting Information for optimised geometries). Similar basis set compositions were already shown to be useful for the description of binding of NO and CO to Fe(II) and Fe(III) systems.[45,63] Second-derivative calculations ensured that the located minima corresponded to stable structures on the PES. At the optimized geometries additional single-point energies were computed, at the DFT (BP86[64,65] and hybrid B3LYP,[66] B3LYP*,[67] and B3PW91[68] functionals including the D3 dispersion correction with BJ damping,) and natural pair orbital-based local DLPNO-CCSD(T0)[69] levels with the zeroth-order relativistic approximation

Chemistry–A European Journal

Research Article
doi.org/10.1002/chem.202200930

**Chemistry
Europe**
European Chemical
Societies Publishing

(ZORA)[70] using the ZORA-def2-TZVP basis set with the Orca 4.2.1. program package.[71,72] For the latter calculations, the coupled-cluster expansion was performed based on the Kohn-Sham orbitals obtained with the BP86 functional. Test calculations using instead B3PW91 orbitals led to almost identical relative energies. Density fitting (RI) approximation was applied with the SARC/J auxiliary basis set in these calculations.

Molecular Dynamics Simulations

The crystal structure coordinates of *Shewanella oneidensis* H-NOX protein for **A**, **B**, and **D** were extracted from the protein data bank under ID numbers 4 U99, 4 U9G and 4 U9B, respectively. They were used as a starting point for MD simulations of the four key structures in the proposed reaction mechanism: **A**, **B**, **D***, and **D**. The structures for **A** and **B** are based on proteins with some point mutations; for the MD study, the corresponding residues were back-mutated to the wild-type amino acids: Gln^{154}Ala/Gln^{155}Ala/Lys^{156}Ala, using the Maestro software package. Under neutral pH, all titratable amino acids were preserved in the same protonation states as predicted by the authors,[39] with the exception of His^{103} in **D**, where we chose to put the proton on δN instead of εN of the histidine ring, due to the fact that His^{103} coordinates to Fe via its εN. The 4 U9G structure representing **B** includes carbon monoxide instead of NO, this was changed manually. The very first step in preparing an MD simulation run is to generate a topology file for the system that contains all the bonded and non-bonded parameters. Therefore, in order to simulate structure **B**, a bond between the nitrogen of the distal NO and Fe(II) of the heme was created. In contrast, in structures **D*** and **D**, there is no bond between the εN of the proximal His^{103} and Fe(II), so the side chain of His^{103} is free to move. Therefore, we ensured that the topology file included no bond between these two fragments. We added the force filed parameters required to simulate these structures into the topology file of the systems (see Supporting Information). Iterative solvation by the optimal point charge (OPC) water model[73] was then performed for all structures; water molecules were arranged in a rhombic dodecahedron box, where the protein was placed at least 12 Å from the box edge. The total charge was neutralized, and physiological concentrations of Na$^+$ and Cl$^-$ ions were set as described in the Supporting Information. The structure of the prepared system was sequentially energy-minimized to diminish unfavourable initial contacts, followed by sequential relaxation of constraints on protein atoms in three NVT steps and an additional NPT (100 ps) simulation to initiate 1 bar pressure. Finally, 150–450 ns MD simulations were performed in the NPT ensemble at 310 K and 1 bar, and without any positional restraints. Snapshots were taken at 4 ps intervals for further analysis. All MD calculations used the CHARMM27 force field and the GROMACS package.[74] The stability of the MD simulations was checked calculating the RMSD of mainchain heavy atoms (i.e. backbone heavy atoms and carbonyl oxygen) along the whole trajectory as well as obtaining its cumulative average.

The diffusion of NO within the protein matrix was investigated in the case of **A** using the previously described methodology.[44,52] First we clustered the structures visited along the MD simulation of **A** based on the conformation of the mainchain heavy atoms. The mid-structure of the most populated cluster for A served as the starting structure for simulation of NO diffusion. We then placed 40 NO molecules, modelled with a three-site model,[75] into solvent-free holes around the protein system and ran an MD simulation for 400 ns. Finally, the occupancy of the distal and proximal pockets by NO was calculated from the equilibrated portion of the trajectory.[53]

QM/MM Calculations

The calculations for the QM and MM regions of the system were performed with two different packages – Gaussian 09[76] and Tinker,[77] respectively. To combine the QM and MM parts of the system as a QM/MM calculation, the QoMMMa program maintained within the Leuven group was employed.[78] In this implementation, QoMMMa uses an additive QM/MM scheme, and at the QM/MM boundary, the valences in the QM region are satisfied using the hydrogen link atom procedure.[79] To mitigate non-physical effects caused by this bridging, the charge on the neighbouring MM atom was set to zero, and its original charge was distributed across adjacent atoms to preserve a neutral charge. For the QM region, all calculations were performed using the BP86 and/or B3LYP functionals with D3 dispersion correction with BJ damping.[61,62] We used the 6–31G*/6-311+G* basis set combination, with the higher accuracy basis set being used to describe the atoms with the greatest electronic structure change – Fe, the four pyrrole nitrogens, and any incoming or bound NO molecules. The MM part of the system was described by the same CHARMM27 forcefield as was used in MD simulations.

The reaction paths leading from **B** to **C** and from **B** to **D*** (see Figure 1) were evaluated using adiabatic mapping. In order to consider the effect of protein conformation on the reaction profiles, three snapshots taken from the MD simulation of **B** were used as starting structures (please see the Supporting Information for a more detailed description of their generation). In order to model the conversion of **B** to **C** an additional NO molecule was placed in the proximal pocket. The reaction coordinate used to drive the transformation of **B** to **D*** was the distance between the heme iron and the εN of His^{103}; all species were modelled as doublets using unrestricted DFT. The reaction coordinate for the reaction path from **B** to **C** was the difference between two distances: (1) the distance between the heme iron and the εN of His^{103} (d(Fe-IM)) representing the breaking of the Fe-His bond (also referred to as the Fe-IM bond below) and (2) the distance (d(Fe-NO)) between the heme Fe and the N of the incoming NO ligand representing formation of the proximal Fe-NO bond. This reaction was studied in the singlet state with care taken to identify and broken symmetry open-shell singlet solutions where these lie lower in energy than the closed-shell solution. Further details regarding the selection of QM and MM regions, and the way in which initial structures were constructed can be found in the Supporting Information.

Conflict of Interest

The authors declare no conflict of interest.

Data Availability Statement

The data that support the findings of this study are available in the supplementary material of this article.

Keywords: bioinorganic chemistry · computational chemistry · molecular dynamics · quantum chemistry · signal transduction

[1] W. R. Montfort, J. A. Wales, A. Weichsel, *Antioxid. Redox Signaling* **2017**, *26*, 107–121.

[2] K. M. Sanders, S. M. Ward, K. D. Thornbury, H. H. Dalziel, D. P. Westfall, A. Carl, *Jpn. J. Pharmacol.* **1992**, *58*, 220–225.

[3] N. B. Fernhoff, E. R. Derbyshire, M. A. Marletta, *Proc. Natl. Acad. Sci. USA* **2009**, *106*, 21602–21607.

[4] D. Hervé, A. Philippi, R. Belbouab, M. Zerah, S. Chabrier, S. Collardeau-Frachon, F. Bergametti, A. Essongue, E. Berrou, V. Krivosic, C. Sainte-Rose, E. Houdart, F. Adam, K. Billiemaz, M. Lebret, S. Roman, S. Passemard, G. Boulday, A. Delaforge, S. Guey, X. Dray, H. Chabriat, P. Brouckaert, M. Bryckaert, E. Tournier-Lasserve, *Am. J. Hum. Genet.* **2014**, *94*, 385–394.

[5] S. Wallace, D. C. Guo, E. Regalado, L. Mellor-Crummey, M. Bamshad, D. A. Nickerson, R. Dauser, N. Hanchard, R. Marom, E. Martin, V. Berka, I. Sharina, V. Ganesan, D. Saunders, S. A. Morris, D. M. Milewicz, *Clin. Genet.* **2016**, *90*, 351–360.

[6] C. Farah, L. Y. M. Michel, J. L. Balligand, *Nat. Rev. Cardiol.* **2018**, *15*, 292–316.

[7] R. Liu, Y. Kang, L. Chen, *Nat. Commun.* **2021**, *12*, 5492.

[8] E. R. Derbyshire, M. A. Marletta, *Annu. Rev. Biochem.* **2012**, *81*, 533–559.

[9] G. Wu, E. Martin, V. Berka, W. Liu, E.D. Garcin, A. L. Tsai, *J. Inorg. Biochem.* **2021**, *214*, 111267.

[10] P. Agvald, L. C. Adding, A. Artlich, M. G. Persson, L. E. Gustafsson, *Br. J. Pharmacol.* **2002**, *135*, 373–382.

[11] Y. Zhao, P. E. Brandish, D. P. Ballou, M. A. Marletta, *Proc. Natl. Acad. Sci. USA* **1999**, *96*, 14753–14758.

[12] E. R. Derbyshire, A. Gunn, M. Ibrahim, T. G. Spiro, R. D. Britt, M. A. Marletta, *Biochemistry* **2008**, *47*, 3892–3899.

[13] E. Martin, V. Berka, I. Sharina, A. L. Tsai, *Biochemistry* **2012**, *51*, 2737–2746.

[14] S. P. L. Cary, J. A. Winger, M. A. Marletta, *Proc. Natl. Acad. Sci. USA* **2005**, *102*, 13064–13069.

[15] N. Sayed, P. Baskaran, X. Ma, F. Van Den Akker, A. Beuve, *Proc. Natl. Acad. Sci. USA* **2007**, *104*, 12312–12317.

[16] V. G. Kharitonov, A. R. Sundquist, V. S. Sharma, *J. Biol. Chem.* **1995**, *270*, 28158–28164.

[17] E. Martin, V. Berka, A. L. Tsai, F. Murad, *Methods Enzymol.* **2005**, *396*, 478–492.

[18] S. J. George, C. R. Andrew, D. M. Lawson, R. N. F. Thorneley, R. R. Eady, ## **2001**, 9683–9684.

[19] S. Louka, S. M. Barry, D. J. Heyes, M. Q. E. Mubarak, H. S. Ali, L. M. Alkhalaf, A. W. Munro, N. S. Scrutton, G. L. Challis, S. P. De Visser, *J. Am. Chem. Soc.* **2020**, *142*, 15764–15779.

[20] J. Lang, A. Maréchal, M. Couture, J. Santolini, *Biophys. J.* **2016**, *111*, 2099–2109.

[21] E. M. Boon, J. H. Davis, R. Tran, D. S. Karow, S. H. Huang, D. Pan, M. M. Miazgowicz, R. A. Mathies, M. A. Marletta, *J. Biol. Chem.* **2006**, *281*, 21892–21902.

[22] G. Wu, W. Liu, V. Berka, A. lim Tsai, *Biochimie* **2017**, *140*, 82–92.

[23] Y. Guo, D. L. M. Suess, M. A. Herzik, A. T. Iavarone, R. D. Britt, M. A. Marletta, *Nat. Chem. Biol.* **2017**, *13*, 1216–1221.

[24] J. R. Stone, M. A. Marietta, *Biochemistry* **1994**, *33*, 5636–5640.

[25] D. Maurer, T. R. Enugala, E. Hamnevik, P. Bauer, M. Lüking, D. Petrović, H. Hillier, S. C. L. Kamerlin, D. Dobritzsch, M. Widersten, *ACS Catal.* **2018**, *8*, 7526–7538.

[26] A. Warshel, R. M. Weiss, *J. Am. Chem. Soc.* **1980**, *102*, 6218–6226.

[27] B. A. Amrein, P. Bauer, F. Duarte, Å. Janfalk Carlsson, A. Naworyta, S. L. Mowbray, M. Widersten, S. C. L. Kamerlin, *ACS Catal.* **2015**, *5*, 5702–5713.

[28] R. Lonsdale, J. N. Harvey, A. J. Mulholland, *Chem. Soc. Rev.* **2012**, *41*, 3025–3038.

[29] X. Sheng, M. Kazemi, F. Planas, F. Himo, *ACS Catal.* **2020**, *10*, 6430–6449.

[30] F. Himo, *J. Am. Chem. Soc.* **2017**, *139*, 6780–6786.

[31] M. R. A. Blomberg, T. Borowski, F. Himo, R. Z. Liao, P. E. M. Siegbahn, *Chem. Rev.* **2014**, *114*, 3601–3658.

[32] S. B. Han, H. S. Ali, S. P. de Visser, *Inorg. Chem.* **2021**, *60*, 4800–4815.

[33] M. G. Quesne, S. P. de Visser, in *Challenges Adv. Comput. Chem. Phys.*, Springer, **2019**, pp. 439–462.

[34] M. J. Field, P. A. Bash, M. Karplus, *J. Comput. Chem.* **1990**, *11*, 700–733.

[35] A. Warshel, M. Levitt, *J. Mol. Biol.* **1976**, *103*, 227–249.

[36] M. G. Quesne, T. Borowski, S. P. De Visser, *Chem. Eur. J.* **2016**, *22*, 2562–2581.

[37] H. Hirao, in *Challenges Adv. Comput. Chem. Phys.*, Springer, **2019**, pp. 463–486.

[38] F. Claeyssens, J. N. Harvey, F. R. Manby, R. A. Mata, A. J. Mulholland, K. E. Ranaghan, M. Schütz, S. Thiel, W. Thiel, H. J. Werner, *Angew. Chem. Int. Ed.* **2006**, *45*, 6856–6859; *Angew. Chem.* **2006**, *118*, 7010–7013.

[39] M. A. Herzik, R. Jonnalagadda, J. Kuriyan, M. A. Marletta, *Proc. Nat. Acad. Sci.* **2014**, *111*, E4156-E4164.

[40] V. K. K. Praneeth, C. Näther, G. Peters, N. Lehnert, *Inorg. Chem.* **2006**, *45*, 2795–2811.

[41] A. Ghosh, *Acc. Chem. Res.* **2005**, *38*, 943–954.

[42] M. Ibrahim, C. Xu, T. G. Spiro, *J. Am. Chem. Soc.* **2006**, *128*, 16834–16845.

[43] M. S. Liao, M. J. Huang, J. D. Watts, *J. Phys. Chem. B* **2013**, *117*, 10103–10114.

[44] L. M. Blomberg, M. R. A. Blomberg, P. E. M. Siegbahn, *J. Inorg. Biochem.* **2005**, *99*, 949–958.

[45] A. Lábas, D. K. Menyhárd, J. N. Harvey, J. Oláh, *Chem. Eur. J.* **2018**, *24*, 5350–5358.

[46] M. Feldt, Q. M. Phung, K. Pierloot, R. A. Mata, J. N. Harvey, *J. Chem. Theory Comput.* **2019**, *15*, 922–937.

[47] D. G. Liakos, Y. Guo, F. Neese, *J. Phys. Chem. A* **2020**, *124*, 90–100.

[48] N. Strickland, J. N. Harvey, *J. Phys. Chem. B* **2007**, *111*, 841–52.

[49] C. Xu, T. G. Spiro, *J. Biol. Inorg. Chem.* **2008**, *13*, 613–621.

[50] D. M. A. Smith, M. Dupuis, E. R. Vorpagel, T. P. Straatsma, *J. Am. Chem. Soc.* **2003**, *125*, 2711–2717.

[51] C. Rovira, K. Kunc, J. Hutter, P. Ballone, M. Parrinello, *J. Phys. Chem. A* **1997**, *101*, 8914–8925.

[52] C. N. Hall, J. Garthwaite, *Nitric Oxide – Biol. Chem.* **2009**, *21*, 92–103.

[53] A. M. Rozza, D. K. Menyhárd, J. Oláh, *Molecules* **2020**, *25*, 1–19.

[54] B. K. Yoo, I. Lamarre, J. L. Martin, F. Rappaport, M. Negrerie, W. A. Eaton, *Proc. Natl. Acad. Sci. USA* **2015**, *112*, E1697-E1704.

[55] R. Banerjee, J. D. Lipscomb, *Acc. Chem. Res.* **2021**, *54*, 2185–2195.

[56] Y. Kang, R. Liu, J. X. Wu, L. Chen, *Nature* **2019**, *5564*, 206–210.

[57] D. J. Stuehr, S. Misra, Y. Dai, A. Ghosh, *J. Biol. Chem.* **2021**, *296*, 100336.

[58] B. Roy, E. J. Halvey, J. Garthwaite, *J. Biol. Chem.* **2008**, *283*, 18841–18851.

[59] R. Radi, *Proc. Natl. Acad. Sci. USA* **2004**, *101*, 4003–4008.

[60] Gaussian 16, M. J. Frisch, G. W. Trucks, H. B. Schlegel, G. E. Scuseria, M. A. Robb, J. R. Cheeseman, G. Scalmani, V. Barone, G. A. Petersson, H. Nakatsuji, X. Li, M. Caricato, A. V Marenich, J. Bloino, B. G. Janesko, R. Gomperts, B. Mennucci, H. P. Hratchian, J. V. Ortiz, A. F. Izmaylov, J. L. Sonnenberg, D. Williams-Young, F. Ding, F. Lipparini, F. Egidi, J. Goings, B. Peng, A. Petrone, T. Henderson, D. Ranasinghe, V. G. Zakrzewski, J. Gao, N. Rega, G. Zheng, W. Liang, M. Hada, M. Ehara, K. Toyota, R. Fukuda, J. Hasegawa, M. Ishida, T. Nakajima, Y. Honda, O. Kitao, H. Nakai, T. Vreven, K. Throssell, J. A. Montgomery Jr., J. E. Peralta, F. Ogliaro, M. J. Bearpark, J. J. Heyd, E. N. Brothers, K. N. Kudin, V. N. Staroverov, T. A. Keith, R. Kobayashi, J. Normand, K. Raghavachari, A. P. Rendell, J. C. Burant, S. S. Iyengar, J. Tomasi, M. Cossi, J. M. Millam, M. Klene, C. Adamo, R. Cammi, J. W. Ochterski, R. L. Martin, K. Morokuma, O. Farkas, J. B. Foresman, D. J. Fox, Gaussian, Inc., Wallingford CT, **2016**.

[61] S. Grimme, J. Antony, S. Ehrlich, H. Krieg, *J. Chem. Phys.* **2010**, *132*, 154104.

[62] S. Grimme, S. Ehrlich, L. Goerigk, *J. Comput. Chem.* **2011**, *32*, 1456–1465.

[63] J. Oláh, J. N. Harvey, *J. Phys. Chem. A* **2009**, *113*, 7338–7345.

[64] A. D. Becke, *Phys. Rev. A* **1988**, *38*, 3098–3100.

[65] J. P. Perdew, K. Burke, M. Ernzerhof, *Phys. Rev. Lett.* **1996**, *77*, 3865–3868.

[66] P. J. Stephens, F. J. Devlin, C. F. Chabalowski, M. J. Frisch, *J. Phys. Chem.* **1994**, *98*, 11623–11627.

[67] M. Reiher, O. Salomon, B. A. Hess, *Theor. Chem. Acc.* **2001**, *107*, 48–55.

[68] A. D. Becke, *J. Chem. Phys.* **1993**, *98*, 5648–5656.

[69] C. Riplinger, F. Neese, *J. Chem. Phys.* **2013**, *138*, 034106.

[70] E. Van Lenthe, E. J. Baerends, J. G. Snijders, *J. Chem. Phys.* **1993**, *99*, 4597–4610.

[71] F. Neese, *Wiley Interdisc. Rev.: Comput. Mol. Sci.* **2012**, *2*, 73–78.

[72] F. Neese, *WIREs Comput. Mol. Sci.* **2018**, *8*, 1327.

[73] S. Izadi, R. Anandakrishnan, A. V. Onufriev, *J. Phys. Chem. Lett.* **2014**, *5*, 3863–3871.

Chemistry–A European Journal

Research Article
doi.org/10.1002/chem.202200930

Chemistry
Europe
European Chemical
Societies Publishing

[74] S. Pronk, S. Pall, R. Schulz, P. Larsson, P. Bjelkmar, R. Apostolov, M. R. Shirts, J. C. Smith, P. M. Kasson, D. van der Spoel, B. Hess, E. Lindahl, *Bioinformatics* **2013**, *29*, 845–854.

[75] M. Meuwly, O. M. Becker, R. Stote, M. Karplus, *Biophys. Chem.* **2002**, *98*, 183–207.

[76] Gaussian 09, M. J. Frisch, G. W. Trucks, H. B. Schlegel, G. E. Scuseria, M. A. Robb, J. R. Cheeseman, G. Scalmani, V. Barone, B. Mennucci, G. A. Petersson, H. Nakatsuji, M. Caricato, X. Li, H. P. Hratchian, A. F. Izmaylov, J. Bloino, G. Zheng, J. L. Sonnenberg, M. Hada, M. Ehara, K. Toyota, R. Fukuda, J. Hasegawa, M. Ishida, T. Nakajima, Y. Honda, O. Kitao, H. Nakai, T. Vreven, J. A. Montgomery Jr., J. E. Peralta, F. Ogliaro, M. Bearpark, J. J. Heyd, E. Brothers, K. N. Kudin, V. N. Staroverov, R. Kobayashi, J. Normand, K. Raghavachari, A. Rendell, J. C. Burant, S. S. Iyengar, J. Tomasi, M. Cossi, N. Rega, J. M. Millam, M. Klene, J. E. Knox, J. B. Cross, V. Bakken, C. Adamo, J. Jaramillo, R. Gomperts, R. E. Stratmann, O. Yazyev, A. J. Austin, R. Cammi, C. Pomelli, J. W. Ochterski, R. L. Martin, K. Morokuma, V. G. Zakrzewski, G. A. Voth, P. Salvador, J. J. Dannenberg, S. Dapprich, A. D. Daniels, Ö. Farkas, J. B. Foresman, J. V Ortiz, J. Cioslowski, D. J. Fox, Gaussian, Inc., Wallingford CT, **2016**.

[77] J. A. Rackers, Z. Wang, C. Lu, M. L. Laury, L. Lagardère, M. J. Schnieders, J. P. Piquemal, P. Ren, J. W. Ponder, *J. Chem. Theory Comput.* **2018**, *14*, 5273–5289.

[78] J. N. Harvey, *Faraday Discuss.* **2004**, *127*, 165–177.

[79] N. Reuter, A. Dejaegere, B. Maigret, M. Karplus, *J. Phys. Chem. A* **2000**, *104*, 1720–1735.